A quantum mechanics/molecular mechanics study of the steric influence of the PR_3 spectator ligands on the energetics of ethylene insertion into the Rh–H bond of $HRh(PR_3)_2(CO)(\eta^2\text{-}CH_2{=}CH_2)$

Stephen A. Decker and Thomas R. Cundari*

Computational Research on Materials Institute (CROMIUM), Department of Chemistry, The University of Memphis, Memphis, TN 38152, USA

Received (in New Haven, CT, USA) 24th July 2001, Accepted 18th September 2001
First published as an Advance Article on the web 8th January 2002

Details of a quantum mechanics/molecular mechanics (QM/MM) study aimed at determining how the substituents of the spectator phosphine ligands influence the energetics of the key step in olefin hydroformylation, the insertion of an olefin into the Rh–H bond of $HRh(PR_3)_2(CO)(\eta^2$-olefin), are discussed. For ethylene there are a total of three insertion pathways originating from the two η^2-ethylene isomers, with either a bis-equatorial arrangement (**ee**) or a mixed equatorial, axial arrangement (**ea**) of the two PR_3 ligands. The energetics, kinetic and thermodynamic, of these three pathways were computed for a variety of phosphine substituents (PR_3; R = Me, ^{t}Bu, Ph, *meta*-$PhSO_3^-$, and *para*-$PhSO_3^-$) using the ONIOM QM/MM approach. These calculations predict that two reaction channels, one originating from the more stable **ea** η^2-ethlyene adduct and the other from the less stable **ee** η^2-ethylene adduct, will be operative for the ethylene insertion reaction with the PMe_3 ligand system, although the latter will be preferred thermodynamically over the former. In the case of the aryl phosphine ligands, a clear energetic preference, kinetically and thermodynamically, was found for ethylene insertion to proceed from the least stable **ee** ethylene adduct *versus* the paths originating from the more stable **ea** ethylene adduct.

The hydroformylation of olefins (*i.e.*, the conversion of an olefin, CO, and H_2 to the corresponding aldehyde) is one of the largest, most important industrial catalytic processes, producing millions of tons of aldehydes annually. As such it has garnered considerable attention from experimental and computational chemists. The widely accepted mechanism for olefin hydroformylation employing the $HRh(PR_3)_2(CO)$ catalyst system was proposed over 30 years ago by Wilkinson *et al.*[1–5] and it is displayed in Scheme 1 for ethylene hydroformylation. The catalytic cycle is comprised of many of the fundamental reactions of organometallic catalysis: oxidative addition/reductive elimination, insertion/elimination, and ligand association/dissociation. Furthermore, the reaction coordinate involves changes in both formal oxidation state and coordination number, and is thus challenging to model. A variety of organometallic compounds have been employed as homogeneous catalysts for olefin hydroformylation, although the phosphine modified Rh carbonyl complexes of the type $HRh(PR_3)_m(CO)_n$ (where $m = 1$ and $n = 2$ or $m = 2$ and $n = 1$) have emerged as the most popular catalysts.

The mechanism of olefin hydroformylation has been the focus of a number of computational studies, as illustrated in the recent review article by Torrent *et al.*[6] Frenking and co-workers have explored the initial catalyst generation step for the $HRh(PR_3)_m(CO)_n$ catalyst systems.[7] Morokuma *et al.* have constructed the entire potential energy hypersurface for ethylene hydroformylation by a $HRh(PH_3)(CO)_2$ model catalyst.[8–12] More recently, our group has investigated the mechanism of ethylene hydroformylation by a $HRh(PH_3)_2(CO)$ model catalyst.[13] Interestingly, experimental evidence has been interpreted in favor of a rate-determining H_2 oxidative addition step,[2,3] while the theoretical studies by our group[13] and Morokuma *et al.*[12] indicated that CO insertion is rate-determining.

The hydroformylation of terminal olefins produces both linear and branched aldehydes, although linear aldehydes are the more desirable industrial product. The rational design and

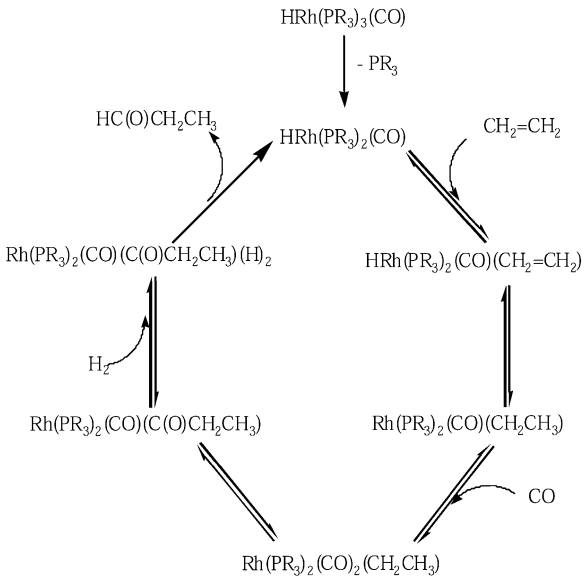

Scheme 1 Wilkinson's catalytic cycle for the hydroformylation of ethylene.

synthesis of transition metal catalysts that provide strict control of aldehyde regiochemistry has become one of the most active areas of research in hydroformylation catalysis.[14,15] The olefin insertion step has been shown to be irreversible, hence this step ultimately determines the regiochemistry of the aldehyde.[16] Not surprisingly, the complex factors governing regioselectivity in olefin hydroformylation have been the subject of a number of theoretical studies,[17–19] including a recent QM/MM study by our group focusing on the insertion of propene into the Rh–H bond of $HRh(PPh_3)_2(CO)(\eta^2$-$CH_2{=}CHCH_3)$.[20]

The current research, which may be considered a corollary to our previous work,[20] employed the ONIOM[21,22] hybrid QM/MM approach to examine how the steric effects of the phosphine substituents (PR_3; where R = Me, ^{t}Bu, Ph, *meta*-$PhSO_3^-$, and *para*-$PhSO_3^-$) influence the energetics of the key olefin insertion step in ethylene hydroformylation. (It should be added that the inclusion of the final two substituents in this study arose from their utility as ligands for the water-soluble olefin hydroformylation process.) Employing ethylene as a model olefin permits a thorough investigation of all possible reaction pathways originating from the two families of isomers of the ethylene adducts [*i.e.*, a bis-equatorial (**ee**) and a mixed equatorial, axial (**ea**) arrangement of the two PR_3 ligands] for the insertion of ethylene into the Rh–H bond of $HRh(PR_3)_2(CO)(\eta^2$-$CH_2{=}CH_2)$. Clearly, the use of ethylene as an olefin prohibits the investigation of regioselectivity in these catalyst systems, however, we feel that the results presented here provide a nice complement to our previous study.

Computational methods

The gas phase potential energy hypersurface for the insertion of ethylene into the RhH bond of $HRh(PR_3)_2(CO)(\eta^2$-$CH_2{=}CH_2)$, for R = Me, ^{t}Bu, Ph, *meta*-$PhSO_3^-$, and *para*-$PhSO_3^-$, was determined using a combined quantum mechanics (QM) and molecular mechanics (MM) approach according to the ONIOM methodology.[21,22] The QM region contained that portion of the molecule at the center of the insertion reaction and was comprised of the rhodium center and its inner coordination sphere, including the entire ethylene unit, that is $HRh(PH_3)_2(CO)(\eta^2$-$CH_2{=}CH_2)$. Density functional theory, employing the B3LYP hybrid density functional (comprised of Becke's hybrid gradient-corrected exchange functional[23] and the gradient-corrected correlation functional of Lee, Yang, and Parr[24]) was employed to model the QM region. In these DFT calculations, the effective core potential (ECP) valence basis set of Stevens *et al.*[25–27] was employed for Rh and the main group atoms. The standard 4-31G contracted basis set was employed for all of the hydrogen atoms in the calculations.[28] This basis set will hereafter be denoted as SBK. The MM region was limited to the bulky R substituents of the two spectator phosphine ligands, and these were modeled with the Universal Force Field (UFF[29]) in the ONIOM calculations. The ONIOM approach employed will hereafter be denoted as B3LYP/SBK:UFF.

Full details of the ONIOM methodology have been described elsewhere,[21,22] thus only a short account of the energy expressions will be given here. In a two-layer ONIOM calculation, such as the DFT:UFF approach employed here, three energies must be calculated: the MM energy of the model system, the QM energy of the model system, and the MM energy of the real system. These three energies are then combined as follows in order to obtain the ONIOM total energy (in this case, the QM energy of the Rh core + the MM energy of the bulky phosphine substituents):

$$E(\text{ONIOM}) = E(\text{QM[model]}) + \{E(\text{MM[real]}) - E(\text{MM[model]})\} \quad (1)$$

Employing the ONIOM approach one can calculate not only the QM/MM combined energy for the real system of interest, but also the gradient of the energy and the Hessian of the energy, needed for the optimization of geometries and the characterization of the resultant stationary points.

The geometries of all species were fully optimized, without any symmetry constraints, using analytical gradient techniques at the B3LYP/SBK:UFF level of theory. For all species, a preliminary conformational search was conducted, keeping the QM Rh core fixed, using the SYBYL force field[30] within the Spartan[31] program prior to submission of the lowest energy conformer to a full ONIOM geometry optimization. All of the resultant optimized stationary points for the η^2-ethylene adducts and the Rh–ethyl insertion products were characterized as minima on their respective potential energy hypersurfaces *via* harmonic vibrational analysis at the B3LYP/SBK:UFF level, using either analytical energy second derivatives or numerical differentiation of the analytical energy first derivatives. Calculation of the harmonic vibrational frequencies for the transition state (TS) species revealed that each contained the single imaginary frequency required to classify it as a true TS. Animation of the normal mode corresponding to this lone imaginary frequency displayed the nuclear motions expected for the ethylene insertion reaction. The Gaussian98 program package[32] was employed for all of the ONIOM calculations. The Opt = NoMicro option within Gaussian98 was employed to aid the convergence of the geometry optimizations.

Results and discussion

The steric influence of the phosphine substituents on the energetics of the olefin insertion step in olefin hydroformylation was investigated in the present work. Employing ethylene as a model substrate, the energetics of the insertion reaction proceeding from the η^2-ethylene adducts, $HRh(PR_3)_2(CO)(\eta^2$-$CH_2{=}CH_2)$, through the various transition states (TSs) and on to the Rh–ethyl products, $Rh(PR_3)_2(CO)(CH_2CH_3)$, were calculated for a variety of phosphine substituents (R) using the ONIOM hybrid QM/MM methodology. The results of these calculations are presented in the following sections.

Previous theoretical studies of the trigonal bipyramidal $HRh(PH_3)_m(CO)_n(\eta^2$-$CH_2{=}CH_2)$ ($m = 1$ and $n = 2$ or $m = 2$ and $n = 1$) models found a strong energetic preference for ethylene to ligate in an equatorial coordination site, with the C=C bond in the equatorial plane.[8,13] Although the increased steric demands of the PR_3 ligands appear to disfavor this parallel coordination mode for ethylene, all of the optimized structures obtained from the current ONIOM calculations revealed that the R groups are directed away from the ethylene ligand. Hence, it appears that the steric destabilization effect will be relatively small and will not override the strong electronic preference for the parallel coordination mode found previously. Given these findings, only structures with this parallel ethylene coordination mode were investigated in the present study. Within this structural motif there are two families of isomers for the η^2-ethylene adducts: one in which the two PR_3 ligands are coordinated in the equatorial position, denoted as **ee**, and another containing an axial PR_3 and an equatorial PR_3 ligand, denoted as **ea**, as shown in Fig. 1.

Proceeding along the reaction coordinate towards the TS, the ethylene ligand rotates out of the equatorial plane and shifts upwards to align the incoming methylene unit with the axial hydride ligand. Interestingly, in the predicted TS structures the ethylene ligand does not complete the rotation to adopt a perpendicular arrangement but rather orients itself intermediate between a perpendicular and parallel alignment. The ethylene insertion reaction originating from the **ee** ethylene adduct goes through a single TS, denoted **ee**‡, due to the C_s pseudo-symmetry of the **ee** isomer. On the other hand, there

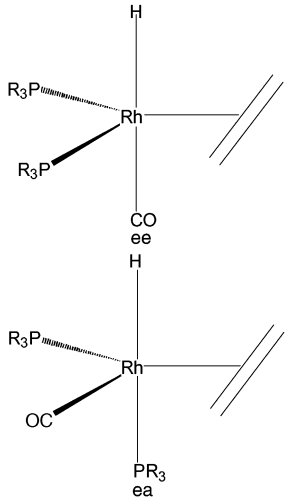

Fig. 1 Schematic representation of the η^2-ethylene adduct isomers, along with the notation adopted in the current paper.

are two possible TSs for the ethylene insertion reaction originating from the **ea** adduct, denoted $\mathbf{ea_1}^{\ddagger}$ and $\mathbf{ea_2}^{\ddagger}$, depending on which direction the ethylene ligand rotates out of the equatorial plane (*i.e.*, with the incoming CH_2 unit directed towards the equatorial PR_3 ligand or towards the equatorial CO ligand). Continuing along the reaction coordinate to the square planar Rh–ethyl insertion products the two PR_3 ligands can be either *cis* or *trans* to one another. These three reaction channels are displayed schematically in Fig. 2. The reaction channels displayed in Fig. 2 were verified previously by our group through the calculated intrinsic reaction coordinates (IRCs) for the analogous ethylene insertion in the PH_3 model catalyst system.[13] Rocha and de Almeida[17] have also corroborated this connectivity *via* IRC calculations for the related propene insertion reaction. Using this scheme as a guideline, the energetics, both kinetic and thermodynamic, for the three possible ethylene insertion reactions were computed for a variety of phosphine co-ligands of varying size (PR_3, where R = Me, ^{t}Bu, Ph, *meta*-$PhSO_3^-$, and *para*-$PhSO_3^-$), the results of which are discussed in the following sections.

Phosphine substituent effects on alkene adduct stability

The relative energies of the **ee** and **ea** isomers of $HRh(PR_3)_2(CO)(\eta^2\text{-}CH_2{=}CH_2)$ for the different phosphine substituents are organized in Table 1. Also included in Table 1 is a decomposition of each ONIOM energy into its quantum mechanics (QM) and molecular mechanics (MM) components. The results indicate an energetic preference of 1–2 kcal mol^{-1} for the **ea** isomer over the **ee** isomer for all of the PR_3 ligands studied. It is interesting to note that the relative ONIOM energies of the **ee** and **ea** isomers are roughly constant for the alkyl/aryl groups investigated. A decomposition of the ONIOM energy reveals that the stability of the **ea** isomer arises from a lower electronic (QM) energy. Interestingly, the energy difference between **ea** and **ee** is very similar for R = Ph and R = *para*-$PhSO_3^-$, indicating that the two substituents possess very similar steric profiles, while the **ea**–**ee** energy difference is slightly larger for R = Me and R = *meta*-$PhSO_3^-$. Also included in Table 1 are the results obtained previously for PH_3 co-ligands.[13] At the B3LYP/SBK(d) level of theory the **ee** and **ea** isomers were predicted to be degenerate. However, a refinement of the energies at the CCSD(T)/SBK(d)//B3LYP/SBK(d) level of theory predicted the **ea** isomer to be

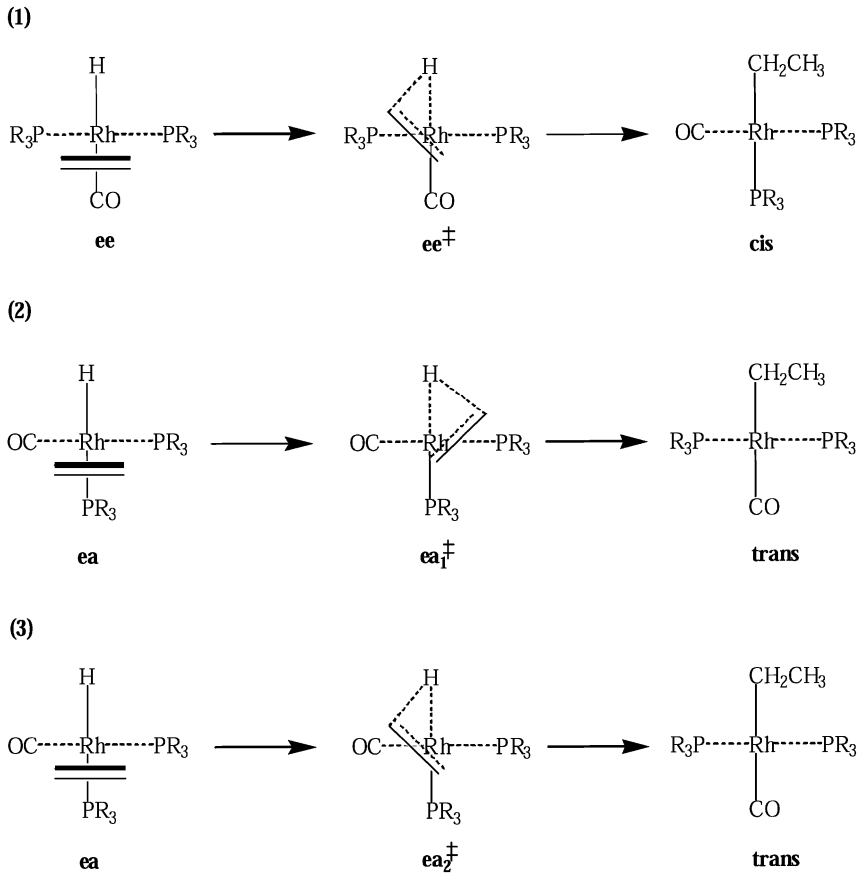

Fig. 2 A schematic representation of the three possible ethylene insertion reaction pathways. The adducts and TSs are viewed along the $Rh\text{–}C{=}C_{centroid}$ bond for illustrative purposes.

Table 1 Summary of the relative energies[a] of the ethylene adducts and decomposition of the ONIOM energy into the QM and MM components

R	E(**ee**)[b]	E_{QM}(**ee**)[c]	E_{MM}(**ee**)[d]	E(**ea**)[b]	E_{QM}(**ea**)[c]	E_{MM}(**ea**)[d]
Me	2.0	1.8	0.2	0.0	0.0	0.0
Ph	1.5	1.5	0.0	0.0	0.0	0.0
m-$PhSO_3^-$	2.4	1.0	1.4	0.0	0.0	0.0
p-$PhSO_3^-$	1.4	1.3	0.1	0.0	0.0	0.0
H[e]	0.0			0.0		
	(1.2)			(0.0)		

[a] All energies are in units of kcal mol^{-1} and are taken relative to the lowest energy isomer. [b] Relative energies computed based on the total ONIOM energies for the real system. They include the zero-point energy corrections and are taken relative to the lowest energy isomer. [c] Relative energies computed based on the energies of the QM region of the molecule [*i.e.*, E_{QM}(model)] and are taken relative to the lowest energy isomer. [d] Relative energies computed based on the energies of the MM region of the molecule [*i.e.*, E_{MM}(real) − E_{MM}(model)] and are taken relative to the lowest energy isomer. [e] Relative energies taken from a previous theoretical study by our group with the model PH_3 ligand taken relative to the lowest energy isomer.[13] The first set of values were computed at the B3LYP/SBK(d) level of theory while those in parentheses correspond to the values computed at the CCSD(T)/SBK(d)//B3LYP/SBK(d) level of theory.

more stable than the **ee** isomer by 1.2 kcal mol^{-1}. Hence, it appears that the electronic preference for **ea** overrides the larger steric crowding between the two PR_3 ligands. The geometry optimizations of the **ee** and **ea** isomers of $HRh(P^tBu_3)_2(CO)(\eta^2\text{-}CH_2{=}CH_2)$ led to the dissociation of one of the P^tBu_3 ligands. Although this prevents us from comparing the results for R = ^{t}Bu, these results do suggest that for extremely bulky phosphine substituents the mono-phosphine, bis-carbonyl catalyst system $[HRh(PR_3)(CO)_2]$ is likely the active catalyst species.

Phosphine substituent effects on transition state stability

The relative energies of the three TS species (**ee**‡, **ea$_1$**‡, and **ea$_2$**‡) for each phosphine substituent studied are displayed in Table 2, along with the QM and MM components of the ONIOM energy. As seen in Table 2, **ea$_1$**‡ is predicted to be the least stable of the three TSs for all of the phosphine substituents studied here, due primarily to its substantially higher electronic energy. This TS isomer was also found to have the highest energy for R = H, supporting the inference that the instability of **ea$_1$**‡ arises primarily from unfavorable electronic interactions.[13] For R = Me, **ea$_2$**‡ is predicted to be slightly more stable than **ee**‡ by 0.7 kcal mol^{-1} due primarily to a lower MM energy. For all of the aryl substituents, the **ee**‡ TS isomer was predicted to be the most stable TS species, lower than **ea$_2$**‡ by 1.3 (Ph), 0.2 (*meta*-$PhSO_3^-$), and 1.7 (*para*-$PhSO_3^-$) kcal mol^{-1} and lower than **ea$_1$**‡ by 3.7 (Ph), 0.7 (*meta*-$PhSO_3^-$), and 4.3 (*para*-$PhSO_3^-$) kcal mol^{-1}. Although, in all cases **ea$_2$**‡ is favored electronically, the larger steric repulsion in **ea$_2$**‡ raises its total energy *versus* the **ee**‡ TS isomer.

Phosphine substituent effects on product stability

The relative energies of the *cis* and *trans* Rh–ethyl insertion products are given in Table 3, along with the partitioning of the ONIOM energies into QM and MM components. From Table 3, the *cis* isomer is preferred energetically over the *trans* isomer by 0.9–5.8 kcal mol^{-1}, for all of the aryl substituents. In each case the *trans* isomer is preferred electronically, however, the overall stability is dictated by the lower steric energy of the *cis* isomer. From the optimized structures it appears that there is a π-stacking type interaction between the phenyl rings of the equatorial PR_3 ligand and the axial PR_3 ligand that acts to stabilize the *cis* isomer for these aryl phosphines, as shown in Fig. 3 for R = *meta*-$PhSO_3^-$. The centroid···centroid distance of the two interacting rings in these *cis* products for the aryl phosphines is ≈ 3.6 Å, which agrees quite well with the available crystal structure data for Rh complexes containing two *cis* PPh_3 ligands, which is of the order of 3.5–3.8 Å.[33] Since the phosphine substituents are described in the MM region, this π-stacking is an MM component of the total energy. A UFF geometry optimization of 2 benzene molecules yields a centroid···centroid distance of 3.5 Å and a binding energy of 5 kcal mol^{-1}, which is more than ample to override the roughly 1–2 kcal mol^{-1} electronic preference for the *trans* isomer. As seen in Table 3 for PMe_3, which has no possible π-stacking interaction, the *trans* isomer is predicted to be more stable than the *cis* isomer, by 1.3 kcal mol^{-1}. This stability arises from the lower QM energy of the *trans* isomer. The results for R = Me agree with those found previously for R = H, which predicted the *trans* isomer to be 1.9 kcal mol^{-1} lower in energy than the *cis* isomer [2.3 kcal mol^{-1} at the CCSD(T)/SBK(d)//B3LYP/SBK(d) level].

Phosphine substituent effects on reaction energetics

The calculated activation barriers (ΔE_a) and thermodynamic energies (ΔE) for the three ethylene insertion reaction channels: **ee** → **ee**‡ → *cis*, **ea** → **ea$_1$**‡ → *trans*, and **ea** → **ea$_2$**‡ → *trans* (see Fig. 2) are summarized in Table 4 for the various phosphine substituents studied here. Also included in Table 4 are the ΔE_a and ΔE values for the three reaction channels

Table 2 Summary of the relative energies[a] of the ethylene insertion transition states and decomposition of the ONIOM energy into the QM and MM components

R	E(**ee**‡)[b]	E_{QM}(**ee**‡)[c]	E_{MM}(**ee**‡)[d]	E(**ea$_1$**‡)[b]	E_{QM}(**ea$_1$**‡)[c]	E_{MM}(**ea$_1$**‡)[d]	E(**ea$_2$**‡)[b]	E_{QM}(**ea$_2$**‡)[c]	E_{MM}(**ea$_2$**‡)[d]
Me	0.7	0.1	0.6	5.2	4.5	0.7	0.0	0.0	0.0
Ph	0.0	0.0	0.0	3.7	3.2	0.6	1.3	− 1.0	2.3
m-$PhSO_3^-$	0.0	0.0	0.0	0.7	4.1	− 3.4	0.2	− 0.9	1.1
p-$PhSO_3^-$	0.0	0.0	0.0	4.3	3.1	1.2	1.7	− 1.0	2.7
H[e]	0.3			4.4			0.0		
	(1.1)			(3.4)			(0.0)		

[a] All energies are in units of kcal mol^{-1} and are taken relative to the lowest energy isomer. [b] Relative energies computed based on the total ONIOM energies for the real system. They include the zero-point energy corrections and are taken relative to the lowest energy isomer. [c] Relative energies computed based on the energies of the QM region of the molecule [*i.e.*, E_{QM}(model)] and are taken relative to the lowest energy isomer. [d] Relative energies computed based on the energies of the MM region of the molecule [*i.e.*, E_{MM}(real) − E_{MM}(model)] and are taken relative to the lowest energy isomer. [e] Relative energies taken from a previous theoretical study by our group with the model PH_3 ligand taken relative to the lowest energy isomer.[13] The first set of values were computed at the B3LYP/SBK(d) level of theory while those in parentheses correspond to the values computed at the CCSD(T)/SBK(d)//B3LYP/SBK(d) level of theory.

Table 3 Summary of the relative energies[a] of the ethylene insertion products and decomposition of the ONIOM energy into the QM and MM components

R	$E(cis)^b$	$E_{QM}(cis)^c$	$E_{MM}(cis)^d$	$E(trans)^b$	$E_{QM}(trans)^c$	$E_{MM}(trans)^d$
Me	1.3	1.2	0.1	0.0	0.0	0.0
Ph	0.0	0.0	0.0	0.9	− 1.3	2.2
m-$PhSO_3^-$	0.0	0.0	0.0	5.8	− 1.6	7.5
p-$PhSO_3^-$	0.0	0.0	0.0	5.2	− 2.4	7.6
H[e]	1.9			0.0		
	(2.3)			(0.0)		

[a] All energies are in units of kcal mol^{-1} and are taken relative to the lowest energy isomer. [b] Relative energies computed based on the total ONIOM energies for the real system. They include the zero-point energy corrections and are taken relative to the lowest energy isomer. [c] Relative energies computed based on the energies of the QM region of the molecule [*i.e.*, E_{QM}(model)] and are taken relative to the lowest energy isomer. [d] Relative energies computed based on the energies of the MM region of the molecule [*i.e.*, E_{MM}(real) − E_{MM}(model)] and are taken relative to the lowest energy isomer. [e] Relative energies taken from a previous theoretical study by our group with the model PH_3 ligand taken relative to the lowest energy isomer.[13] The first set of values were computed at the B3LYP/SBK(d) level of theory while those in parentheses correspond to the values computed at the CCSD(T)/SBK(d)//B3LYP/SBK(d) level of theory.

calculated previously by our group for the model PH_3 ligand systems.[13]

Thermodynamics. An examination of the calculated thermodynamics for the ethylene insertion reaction reveals a preference for **ee** → *cis* (reaction 1 in Fig. 2) over **ea** → *trans* (reactions 2 and 3 in Fig. 2) for all of the substituents studied here. For R = Me and R = Ph both of the reaction channels are predicted to be exothermic, with the **ee** → *cis* pathway predicted to be more exothermic, by 2.0 and 1.6 kcal mol^{-1}, respectively, than the **ea** → *trans* pathways. For the two $PhSO_3^-$ substituents the **ee** → *cis* reaction channel is predicted to be exothermic (by 6.6 kcal mol^{-1} for *meta*-$PhSO_3^-$ and 5.6 kcal mol^{-1} for *para*-$PhSO_3^-$) while the **ea** → *trans* channel is predicted to be slightly endothermic (by 0.8 kcal mol^{-1} for *meta*-$PhSO_3^-$ and 0.1 kcal mol^{-1} for *para*-$PhSO_3^-$). Hence, the substitution of the phenyl rings with sulfonate groups is predicted by the ONIOM calculations to lead to a large thermodynamic preference for the *cis* product.

Kinetics. For the PMe_3 ligands, a slight energetic preference of 0.7 kcal mol^{-1} was predicted for the ethylene insertion reaction to proceed along reaction channel 1 (*cis* product) as opposed to reaction channel 3 (*trans* product), while the barrier for reaction channel 2 was found to be substantially higher (by 5.9 kcal mol^{-1}). However, given the small difference between the energy barriers for these two preferred reaction pathways, it is likely that pathways 1 and 3 will be operative for the ethylene insertion reaction. Hence, for R = Me there does not appear to be a kinetic preference for the ethylene insertion reaction to proceed from either the **ee** or **ea** ethylene adduct. These results are similar to those found previously for the PH_3 model ligand system, which predicted the barriers for reaction paths 1 and 3 to be nearly equivalent, at 13.4 and 13.1 kcal mol^{-1}, respectively [16.6 kcal mol^{-1} for both channels at the CCSD(T)/SBK(d)//B3LYP/SBK(d) level], and much lower than that predicted for pathway 2, at 17.5 kcal mol^{-1} [20.0 kcal mol^{-1} at the CCSD(T)/SBK(d)//B3LYP/SBK(d) level].[13] However, the same cannot be said for the aryl substituents. For R = Ph, *meta*-$PhSO_3^-$, and *para*-$PhSO_3^-$ the energy barrier for ethylene insertion following reaction channel 1 was predicted to be significantly lower, by 2–3 kcal mol^{-1}, than the reaction following channel 3, while the barrier for reaction channel 2 was even larger, by 4–5 kcal mol^{-1}. Hence, the present calculations predict a clear energetic preference for the ethylene insertion reaction to proceed from the **ee** ethylene adduct (leading to the *cis* ethyl product) over the **ea** adduct (leading to the *trans* ethyl product) for the aryl phosphine ligands studied here.

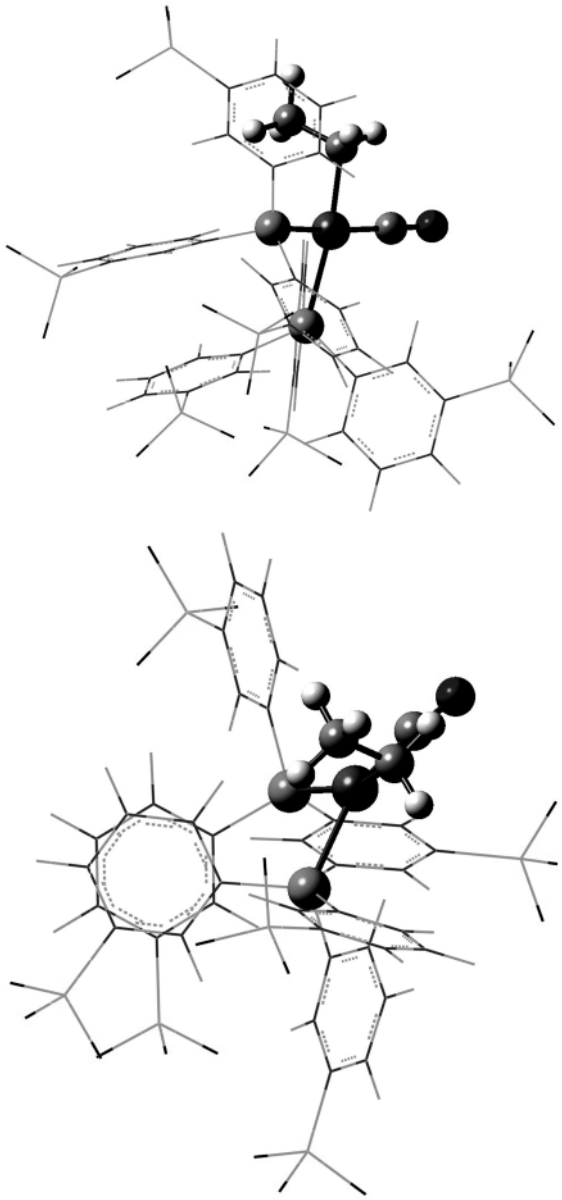

Fig. 3 ONIOM optimized geometric structure of the *cis* isomer of the Rh–ethyl insertion product, $HRh[P(meta\text{-}PhSO_3^-)_3]_2(CO)(CH_2CH_3)$. Two views are given, one looking side-on at the two interacting phenyl rings and the other looking at the two rings from the top.

Table 4 Summary of the calculated ethylene insertion activation barriers (ΔE_a) and thermodynamic energies (ΔE)[a]

R	Activation barrier $\Delta E_a(i)$[b]			Thermodynamic energy $\Delta E(i)$[c]	
	$\Delta E_a(1)$	$\Delta E_a(2)$	$\Delta E_a(3)$	$\Delta E(1)$	$\Delta E(2)$
Me	15.5	21.4	16.2	−3.1	−1.1
Ph	11.7	16.5	14.3	−3.8	−2.2
m-$PhSO_3^-$	13.3	18.1	15.6	−6.6	0.8
p-$PhSO_3^-$	11.6	16.6	14.2	−5.6	0.1
H[d]	13.4	17.5	13.1	−4.8	−6.8
	(16.6)	(20.0)	(16.6)	(−0.6)	(−1.8)

[a] All energies are in units of kcal mol^{-1}. They were computed based on the ONIOM energies of the various species involved and they include the zero-point energy correction. [b] Activation barriers were calculated based on the ONIOM energies of the adducts and the TS species and they include the zero-point energy correction. The index *i* refers to the numbering scheme of the ethylene insertion reaction pathways adopted in Fig. 2 (*i.e.*, $i=1$ for **ee** → **ee**‡ → *cis*, $i=2$ for **ea** → **ea$_1$**‡ → *trans*, and $i=3$ for **ea** → **ea$_2$**‡ → *trans*). [c] Thermodynamic energies were calculated based on the ONIOM energies of the adducts and the Rh–ethyl insertion products and they include the zero-point energy correction. The index *i* refers to the numbering scheme of the ethylene insertion reaction pathways adopted in Fig. 2 (*i.e.*, $i=1$ for **ee** → *cis* and $i=2$ for **ea** → *trans*). [d] Activation barriers and thermodynamic energies taken from a previous theoretical study in our group employing the model PH_3 ligand.[13] The first set of values were computed at the B3LYP/SBK(d) level of theory while those in parentheses correspond to the values computed at the CCSD(T)/SBK(d)//B3LYP/SBK(d) level of theory.

Summary and conclusions

The current work employed the ONIOM QM/MM methodology to examine how the substituents of the spectator phosphine ligands (PR_3) influence the energetics of the key step in olefin hydroformylation, that is the olefin insertion step. Using ethylene as a model olefin, the energetics, both kinetic and thermodynamic, of the three possible ethylene insertion reaction pathways were computed for a variety of phosphine substituents (PR_3 where R = Me, ^{t}Bu, Ph, *meta*-$PhSO_3^-$, and *para*-$PhSO_3^-$).

All geometry optimizations for R = ^{t}Bu resulted in dissociation of one of the P^tBu_3 ligands, suggesting that the less sterically crowded $HRh(P^tBu_3)(CO)_2$ may be the active species in the olefin hydroformylation process, instead of the $HRh(P^tBu_3)_2(CO)$ complex being investigated here.

The results of the current study indicated an energetic preference, of 1–2 kcal mol^{-1}, for the η^2-ethylene adduct with a mixed equatorial, axial disposition of the two PR_3 ligands over the bis-equatorial isomer for the remaining phosphine substituents studied. A comparison of the energies of the two possible Rh–ethyl products, with PR_3 ligands either *cis* or *trans*, revealed an energetic preference for the *trans* arrangement when R = Me, due to a lower electronic energy, and an energetic preference for the *cis* arrangement when R was one of the aryl substituents, due to its lower MM energy. Although this latter results seems somewhat misleading, it can be rationalized by the existence of a stabilizing π-stacking interaction between the phenyl rings of the equatorial and axial phosphine ligands.

A comparison of the computed activation barriers for the three ethylene insertion reaction pathways reveals that the barrier for pathway 2 (**ea** → **ea$_1$**‡ → *trans*) is significantly higher (by 2–5 kcal mol^{-1}) than that predicted for the two alternative reaction pathways (**ee** → **ee**‡ → *cis* and **ea** → **ea$_2$**‡ → *trans*) for all of the phosphine substituents studied, in agreement with the results obtained previously for the PH_3 model system. For R = Me the activation barrier for pathway 1 (**ee** → **ee**‡ → *cis*) was predicted to be slightly smaller, by 0.7 kcal mol^{-1}, than that predicted for pathway 3 (**ea** → **ea$_2$**‡ → *trans*). Furthermore, reaction 1 was predicted to be more exothermic (by 2 kcal mol^{-1}) than reaction channel 3 for the PMe_3 system. However, since the difference in activation barriers is quite small, in all likelihood both reaction channels will be operative for the ethylene insertion reaction in this catalyst system. These results are in line with those found previously for the PH_3 model system.[13] For the arylphosphine ligands studied the activation barrier for reaction channel 1 (**ee** → **ee**‡ → *cis*) was predicted to be significantly smaller, by 2–3 kcal mol^{-1}, than that found for reaction channel 3 (**ea** → **ea$_2$**‡ → *trans*). A comparison of the computed thermodynamic energies for the **ee** → *cis* and **ea** → *trans* paths reveals that the former path is predicted to be more exothermic, by 2–7 kcal mol^{-1}, than the latter path for all of the arylphosphines studied. Hence, in the case of the arylphosphine co-ligands a clear energetic preference, both kinetic and thermodynamic, was found for ethylene insertion to proceed from the least stable **ee** ethylene adduct to the **ee**‡ TS and then to the most stable *cis* Rh–ethyl insertion product.

Acknowledgements

The authors wish to acknowledge support of this research by the United States Department of Energy (grant no. DE-FG02-97ER14811). S. A. D. wishes to thank the Natural Sciences and Engineering Research Council of Canada for financial support through a Postdoctoral Fellowship. This research was performed in part using the Molecular Science Computing Facility (MSCF) in the William R. Wiley Environmental Molecular Sciences Laboratory at the Pacific Northwest National Laboratory. The MSCF is funded by the Office of Biological and Environmental Research in the U.S. Department of Energy. Pacific Northwest is operated by Battelle for the U.S. Department of Energy under contract DE-AC06-76RLO 1830. The authors would also like to acknowledge the National Center for Supercomputing Applications for a CPU allotment on the high performance computing facility at the University of Kentucky and the Department of Defense for an allotment of CPU time on the Maui High Performance Computing Center facility. The authors also acknowledge Prof. Feliu Maseras (UA Barcelona) for communicating the results of his research prior to publication.

References

1 J. A. Osborn, G. Wilkinson and J. F. Young, *Chem. Commun.*, 1965, 17.
2 D. Evans, J. A. Osborn and G. Wilkinson, *J. Chem. Soc. A*, 1968, 3133.
3 D. Evans, G. Yagupsky and G. Wilkinson, *J. Chem. Soc. A*, 1968, 2660.
4 G. Yagupsky, C. K. Brown and G. Wilkinson, *J. Chem. Soc. A*, 1970, 1392.

5 C. K. Brown and G. Wilkinson, *J. Chem. Soc. A*, 1970, 2753.
6 M. Torrent, M. Sola and G. Frenking, *Chem. Rev.*, 2000, **100**, 439.
7 R. Schmid, W. A. Herrmann and G. Frenking, *Organometallics*, 1997, **16**, 701.
8 N. Koga, S. Q. Jin and K. Morokuma, *J. Am. Chem. Soc.*, 1988, **110**, 3417.
9 N. Koga and K. Morokuma, *Top. Phys. Organomet. Chem.*, 1989, **3**, 1.
10 D. G. Musaev, T. Matsubara, A. M. Mebel, N. Koga and K. Morokuma, *Pure Appl. Chem.*, 1995, **67**, 257.
11 D. G. Musaev and K. Morokuma, in *Advances in Chemical Physics*, ed. I. Prigogine and S. A. Rice, Wiley, New York, 1996, p. 61.
12 T. Matsubara, N. Koga, Y. Ding, D. G. Musaev and K. Morokuma, *Organometallics*, 1997, **16**, 1065.
13 S. A. Decker and T. R. Cundari, *Organometallics*, 2001, **20**, 2827.
14 J. P. Collman, L. S. Hegedus, J. R. Norton and R. G. Finke, *Principles and Applications of Organotransition Metal Chemistry*, University Science Books, Mill Valley, CA, 1987.
15 R. H. Crabtree, *The Organometallic Chemistry of the Transition Metals*, Wiley, New York, 1988.
16 C. P. Casey and L. M. Petrovich, *J. Am. Chem. Soc.*, 1995, **117**, 6007.
17 W. R. Rocha and W. B. de Almeida, *Int. J. Quantum Chem.*, 2000, **78**, 42.
18 D. Gleich, R. Schmid and W. A. Herrmann, *Organometallics*, 1998, **17**, 4828.
19 J. J. Carbo, F. Maseras, C. Bo and P. W. N. M. van Leeuwen, *J. Am. Chem. Soc.*, 2001, **123**, 7630.
20 S. A. Decker and T. R. Cundari, *J. Organomet. Chem.*, 2001, **635**, 132.
21 M. Svensson, S. Humbel, R. D. J. Froese, T. Matsubara, S. Sieber and K. Morokuma, *J. Phys. Chem.*, 1996, **100**, 19 357.
22 S. Dapprich, I. Komaromi, K. S. Byun, K. Morokuma and M. J. Frisch, *THEOCHEM*, 1999, **461–462**, 1.
23 A. D. Becke, *J. Chem. Phys.*, 1993, **98**, 5648.
24 C. Lee, W. Yang and R. G. Parr, *Phys. Rev. B.*, 1988, **37**, 785.
25 W. J. Stevens, H. Basch and M. Krauss, *J. Chem. Phys.*, 1984, **81**, 6026.
26 W. J. Stevens, H. Basch, M. Krauss and P. Jasien, *Can. J. Chem.*, 1992, **70**, 612.
27 T. R. Cundari and W. J. Stevens, *J. Chem. Phys.*, 1993, **98**, 5555.
28 R. Ditchfield, W. J. Hehre and J. A. Pople, *J. Chem. Phys.*, 1971, **54**, 724.
29 A. K. Rappe, C. J. Casewit, K. S. Colwell, W. A. Goddard III and W. M. Skiff, *J. Am. Chem. Soc.*, 1992, **114**, 10 024.
30 M. Clark, R. D. Cramer III and N. van Opdensch, *J. Comput. Chem.*, 1989, **10**, 982.
31 W. J. Hehre, W. W. Huang, P. E. Klunzinger, B. J. Deppmeier and A. J. Driessen, *A Spartan Tutorial*, Wavefunction, Inc., Irvine, CA, 1997.
32 M. J. Frisch, G. W. Trucks, H. B. Schlegel, G. E. Scuseria, M. A. Robb, J. R. Cheeseman, V. G. Zakrzewski, J. A. Montgomery, R. E. Sratmann, J. C. Burant, S. Dapprich, J. M. Millam, A. D. Daniels, K. N. Kudin, M. C. Strain, O. Farkas, J. Tomasi, V. Barone, M. Cossi, R. Cammi, B. Mennucci, C. Pomelli, C. Adamo, S. Clifford, J. Ochterski, G. A. Petersson, P. Y. Ayala, Q. Cui, K. Morokuma, D. K. Malick, A. D. Rabuck, K. Raghavachari, J. B. Foresman, J. Cioslowski, J. V. Ortiz, B. B. Stefanov, G. Liu, A. Liashenko, P. Piskorz, I. Komaromi, R. Gomperts, R. L. Martin, D. J. Fox, T. Keith, M. A. Al-Laham, C. Y. Peng, A. Nanayakkara, C. Gonzalez, M. Challacombe, P. M. W. Gill, B. Johnson, W. Chen, M. W. Wong, J. L. Andres, C. Gonzalez, M. Head-Gordon, E. S. Replogle, J. A. Pople, Gaussian98, Pittsburgh, PA, 1998.
33 F. H. Allen and O. Kennard, *Chem. Design Autom. News*, 1993, **8**, 31.